Phase Decomposition of Rapidly Solidified Fe-Mn-Al-C Austenitic Alloys

KWAN H. HAN and WOONG K. CHOO

The phase decomposition of two $(Fe_{0.65}Mn_{0.35})_{0.83}Al_{0.17}$-$xC$ (x = 3 and 4 at. pct or x = 0.74 and 0.98 wt pct) austenitic alloys prepared by rapid solidification (RS) has been investigated on aging at 823 and 923 K by means of X-ray diffraction, transmission electron microscopy, and scanning electron microscopy. Under low bulk carbon supersaturation conditions (823 K aging of low carbon alloy and 923 K aging of high carbon alloy), zones formed preferentially at the cellular boundaries and in the bands in the {100} planes, giving rise to line broadening in the X-ray diffraction patterns. On the other hand, the initial aging under high, carbon supersaturation condition (823 K aging of high carbon alloy) resulted in the sideband formation, resulting from homogeneous structural modulation in the $\langle 100 \rangle_\gamma$ directions throughout the grain. The bulk carbon supersaturation dependence of initial decomposition modes indicates that carbon atom fluctuations are crucial in the initial state of phase decomposition, and that the observed {100} modulated structure corresponds to a structure consisting of alternate carbon-rich and carbon-poor zones. Together with the interstitial clustering process, an fcc-based substitutional ordering reaction concurrently took place. Later on, these zones were replaced by a coherent metastable phase in the matrix, which was finally transformed into the cubic carbide (κ carbide) of $(Fe,Mn)_3AlC_x$ chemical formula with the $L'1_2$ structure. However, at the end, a combined heterogeneous β-Mn and κ carbide precipitation seemed to finalize the decomposition process over the matrix κ carbide precipitation.

I. INTRODUCTION

EVER since the pioneering works of Ham and Cairns[1] and of Schmatz,[2] Fe-Mn-Al-C austenitic alloys, being attracted as strategic element-free potential substitutes for the traditional Fe-Ni-Cr austenitic stainless steels,[3,4] have been touted by several investigators[5,6,7] as a new class of structural steels possessing the age-hardening property. Age hardening in Fe-Mn-Al-C austenitic alloys was previously reported by James[5] and Kayak[6] to occur in the course of isomorphous precipitation of κ carbide of $(Fe,Mn)_3AlC_x$ chemical formula with ordered $L'1_2$ crystal structure (filled-$AuCu_3$) from the supersaturated austenitic phase. Following these reports, an in-depth aging investigation was carried out by Krivonogov *et al.*[8] They studied conventionally prepared Fe-28 wt pct Mn-9 wt pct Al-0.9 wt pct C alloy by means of magnetic measurements, hardness tests, transmission electron microscopy (TEM), and X-ray diffractometry. In that work, they reported the observation of a modulated structure that formed in the initial decomposition stage during aging at 723 to 923 K. The modulation was in the $\langle 100 \rangle_\gamma$ direction. They also examined the overall sequence of the decomposition process, but, unfortunately, the fine details of interpretation of their experimental results were lacking. For this reason, Storchak and Drachinskaya[9] subsequently re-examined the structural changes of the same alloy during aging at 723 to 923 K by rotating crystal X-ray diffraction of a single crystal specimen, in which they observed the sideband phenomenon in the initial stage of aging, supporting previous Krivonogov *et al.*'s TEM observation of the {100} modulated structure. Storchak and Drachinskaya attributed the sideband phenomenon to the modulated structure consisting of carbon-rich and carbon-poor zones. In the next stage, a coherent metastable phase was observed to replace the modulated structure.* But the equilibrium κ carbide precipitation was observed to occur *via* heterogeneous reaction at temperatures above 923 K, and brittle β-Mn phase also precipitated after prolonged aging.[8,9] Storchak and Drachinskaya, however, failed to present the evidence of fluctuations of interstitial carbon atoms in the early stage of decomposition.

Aside from the conventional quenching of Fe-Mn-Al-C alloys as mentioned above, a rapid solidification (RS) technique has been employed by Inoue *et al.*[10] and the present authors[11,12] for alloy preparation. These authors have shown[12] that a single austenitic phase can be obtained in a wide carbon composition range up to 1.65 wt pct C in high manganese (31 wt pct Mn) and aluminum (9 wt pct Al) alloys by the RS technique. It was also shown[11] that the sideband phenomenon occurred during aging of some RS alloys as well. In addition, equilibrium phase stability of RS alloys containing 0 to 4.3 wt pct C was investigated.[12] In the latter work, it was shown that the κ carbide substituted for M_3C and

*There has been some disagreement in designation of the coherent metastable phase: Krivonogov *et al.*[8] used notation K_0 or sometimes ordered K in designating all the coherent precipitates, regardless of the solute-rich zone and the metastable phase. Storchak and Drachinskaya[9] later denoted it as coherent metastable K phase. In order to avoid some confusion, a unified designation seems necessary. We hereby propose a designation, κ', for the coherent metastable phase which forms prior to precipitation of κ carbide.

KWAN H. HAN is Assistant Professor, Department of Metallurgical Engineering, Yeungnam University, Gyongsan, Kyongbuk, Korea. WOONG K. CHOO is Professor, Department of Materials Science and Engineering, Korea Advanced Institute of Science and Technology, P.O. Box 131, Seoul, Korea.

Manuscript submitted May 6, 1985.

$M_{23}C_6$ carbides as an equilibrium carbide phase at temperatures above 823 K. In the end, three different types of decomposition reactions, resulting in either α (ferrite) + β-Mn, $\kappa + \alpha$, or $\kappa + \gamma$, were observed to occur depending on the carbon composition and heat-treating temperature.

The prime motive of this paper is to track down the sequence and to understand the nature of phase decomposition when carbon composition and aging temperature are chosen as variables. The RS technique was chosen as the sample preparation technique for a simple reason: to secure a single austenitic phase otherwise unobtainable by conventional means. As will be shown later, the fine details of microstructure, often camouflaged, of the austenitic RS specimens are different, depending on the carbon content of the alloys. The morphological change of the microstructure is greatly influenced by stability of the austenite phase, which in turn is enhanced by the increased carbon content.

II. EXPERIMENTAL

Two RS alloys of Fe-31.7 wt pct Mn-8.9 wt pct Al-0.74 wt pct C [$(Fe_{0.65}Mn_{0.35})_{0.83}Al_{0.17}$-3 at. pct C: alloy A] and Fe-31.6 wt pct Mn-8.9 wt pct Al-0.98 wt pct C [$(Fe_{0.65}Mn_{0.35})_{0.83}Al_{0.17}$-4 at. pct: alloy B] were chosen for this study. The details of alloy preparation and RS procedure by a gas-tight melt spinner are described in a previous work.[12] The RS alloys were in the shape of long ribbons with the dimensions of about 25 μm in thickness and 3.7 mm in width.

Aging treatments were administered at 823 K in a salt bath and at 923 K in a vertical tube furnace. Specimens cut from the RS ribbons were encapsulated in pyrex or vycor tubes in vacuum prior to aging. X-ray diffraction was performed by a Philips diffractometer equipped with curved crystal-diffracted beam monochromator and Cu-K_α radiation. The microstructures of as-RS and aged alloys were examined by both a SEM equipped with an energy dispersive X-ray analyzer (EDXA) and a Hitachi 100 kV TEM. For SEM examination, specimens were electropolished in a solution consisting of 350 parts ethanol, 50 parts glycerol, 40 parts perchloric acid, and 60 parts distilled water, and then etched in 5 pct nital. For TEM observation, thin foils were prepared, by twin-jet polishing at 253 K, in a solution consisting of 60 parts perchloric acid, 600 parts methanol, and 340 parts buthanol.

III. RESULTS

A. *Structure of As-RS Alloys*

As reported previously,[12] X-ray diffraction patterns of both RS alloys revealed a single austenite phase. Figure 1 shows corresponding melt-spun microstructures taken by SEM after etching, in which it is noted that the solidification structures are not the same; there is the presence of a fine cellular dendritic structure with cell width ranging from a submicron to about 1 μm inside the austenite grains in alloy A (Figure 1(a)), but it is of a homogeneous grain structure in alloy B (Figure 1(c)). Transmission electron (TE) micrograph reveals no other trace-phase, even in RS alloys A and B as shown in Figures 1(b) and (c). Most of the cells in alloy A were observed to have grown in a direction normal to the chill-block surface, but cells elongated along the chill-block surface were occasionally observed in certain areas which did not experience direct contact with chill-block, indicating the occurrence of cell growth parallel to the chill-block surface at these lift-off regions.[13] The grain size of both RS alloys ranged from 1 to 7 μm.

B. *Aging Responses*

1. *Alloy A*

Sequential changes in X-ray diffraction patterns on aging at 823 K are shown in Figure 2. Two distinctly

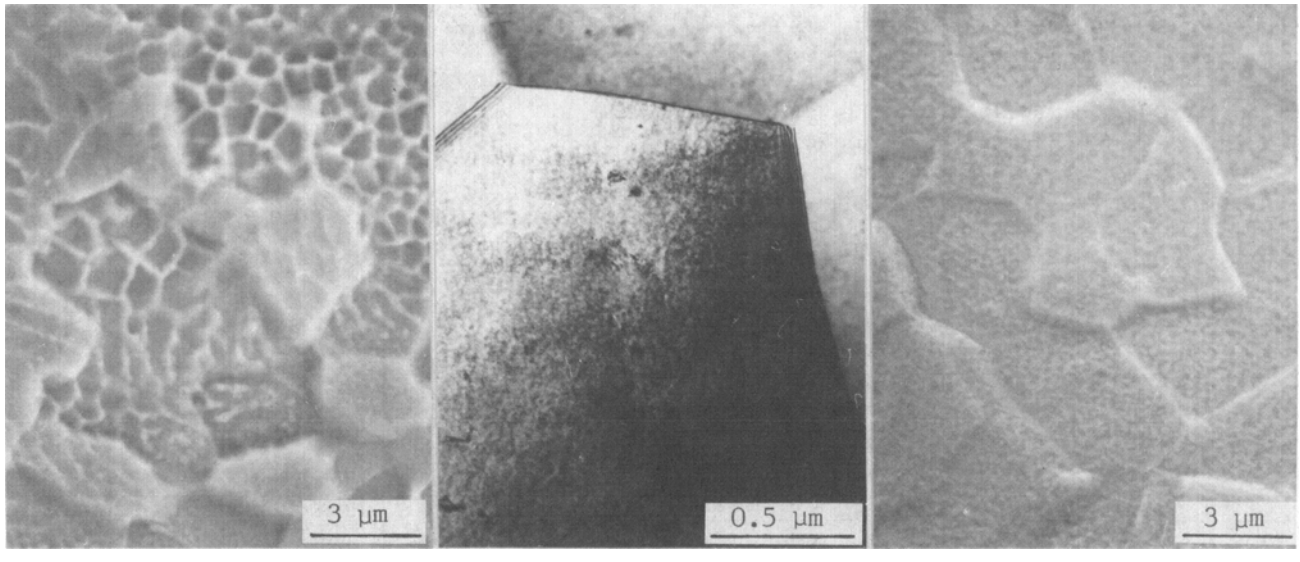

(*a*) (*b*) (*c*)

Fig. 1—Microstructures of as-RS alloys: (*a*) scanning electron micrograph; (*b*) bright-field transmission electron micrograph of alloy A; (*c*) scanning electron micrograph of alloy B.

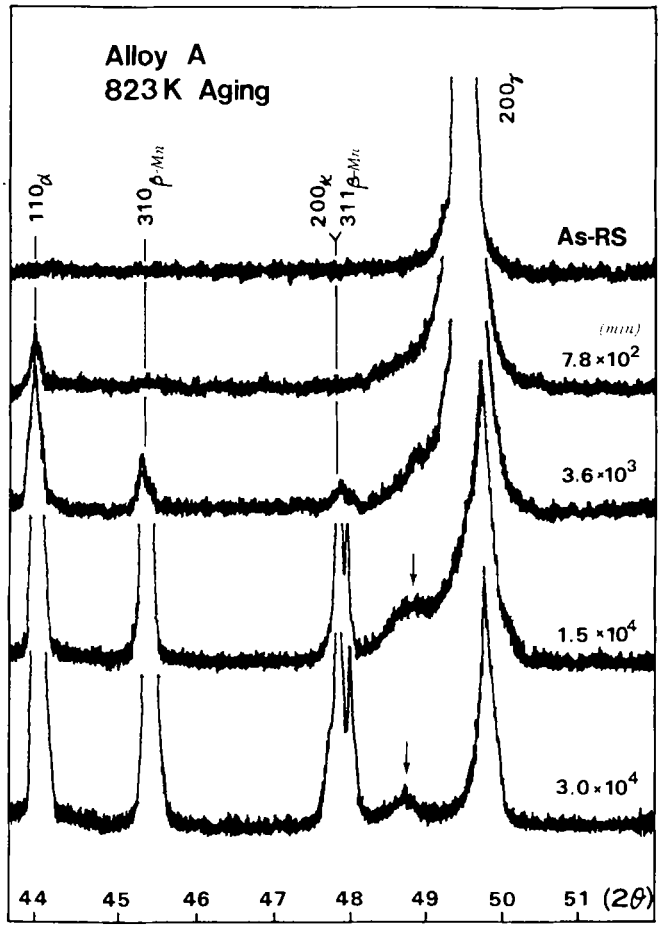

Fig. 2—Sequential changes in the X-ray diffraction pattern of alloy A on aging at 823 K. Arrows indicate the diffraction lines of metastable κ' phase.

different types of development of diffraction lines during phase decomposition can be noted. The first is the diffuse reflection corresponding to an asymmetric line broadening of the parent austenite diffraction line, which later develops another diffraction line at the low-angle side; the second is the development of fairly sharp diffraction lines arising from formation of α, β-Mn, and κ carbide phases. The early development indicates the coherent isomorphous decomposition of parent austenite phase in the matrix, whereas the later development arises from heterogeneous grain boundary precipitation.

The X-ray line broadening observed in this study seems similar to the behavior which had been observed for an age-hardenable Al-Cu alloy,[14] in that there appeared no distinct diffuse maxima like the sideband reflections[9,11] around the main diffraction lines. This suggests that zones are likely to form in the matrix in an aperiodic manner.[15] However, direct TEM observation reveals more complicated featural changes stemming from solute segregation in the as-RS specimen (Figure 1(a)). As can be seen in Figure 3, various image features stand out in a specimen aged for 1.8×10^3 minutes. It is observed in Figure 3(a) that zones have formed preferentially along the intercellular regions of the solidification structure. An interesting, but unfamiliar, feature of the aged microstructure around the intercellular regions is that, as can be noted from that of the upper-left grain in Figure 3(a), it resembles a modulated structure,[16,17] revealing cross-hatched contrast in the $\langle 100 \rangle_\gamma$ directions. A micrograph in Figure 3(b) at higher magnification reveals the finer details of aged microstructure in the vicinity of intercellular region. It was taken from the same foil, using an operating g_{200} in the (002) matrix plane.

The TE micrograph shows a wave-like feature perpendicular to the operating g_{200} in the interior of an intercellular region, but in the outer region rather discrete precipitates are seen. This peculiar image may be ascribed to zone formation, and indicates that the zone size as well as inter-zone distance differs from region to region inside the intercellular region. Zone density is higher in the interior of the intercellular region than in the exterior. Selected area diffraction patterns consistently show

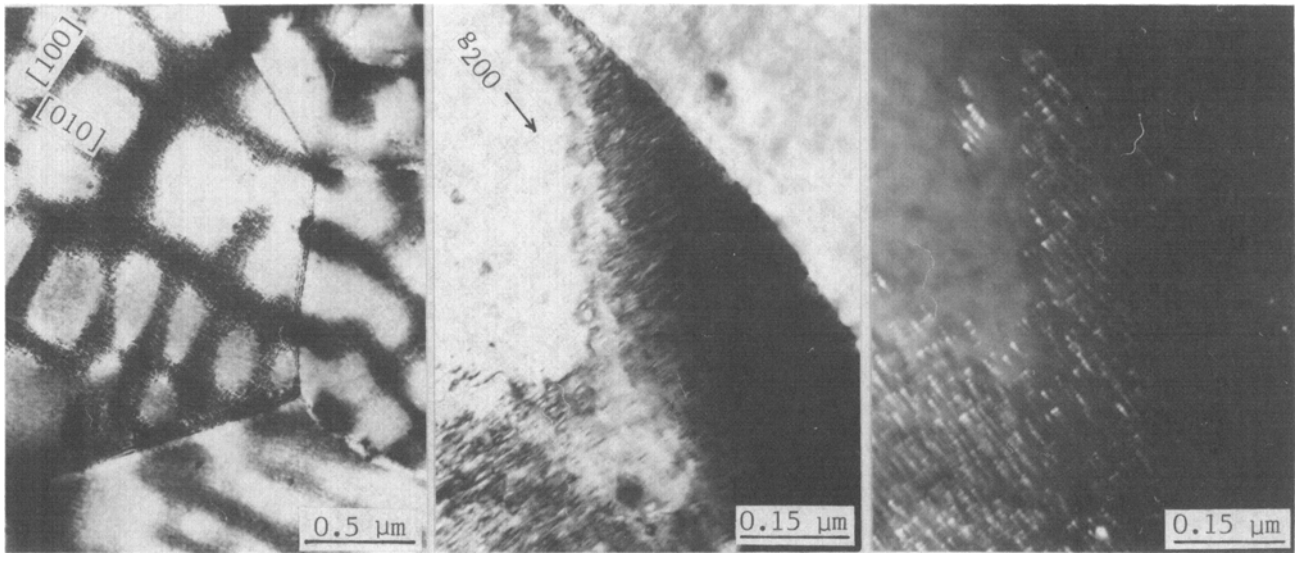

(a) (b) (c)

Fig. 3—Transmission electron micrographs of alloy A after aging at 823 K for 1.8×10^3 min: (*a*) low magnification bright-field image; (*b*) high magnification bright-field image; (*c*) dark-field image of (b) taken from the (100) superlattice spot. Foil normal of (b) and (c) near [001].

superlattice reflections of the ordered fcc-base structure, indicating that ordering has occurred during aging in the solute-rich zones. Figure 3(c) shows a dark-field TE image of Figure 3(b) from the (100) superlattice spot, in which cuboidal zones are seen.

On further aging for 6.7×10^3 minutes, a separate set of diffraction lines begin to appear at the low-angle side of the parent austenite line which at the same time shifts toward the higher-angle side. Such a shift indicates depletion of solute atoms in the matrix. The precipitate phase responsible for the separate diffraction line is found to be of the ordered fcc-base crystal structure using superlattice TE reflections superimposed on fcc fundamental spots. Its lattice parameter is 0.3723 nm, and it then increases to 0.3736 nm after 3.7×10^4 minutes of aging in good agreement with the previous data of the κ' phase.[8,9] Figure 4 shows rafts of the κ' phase precipitated on aging for 1.5×10^4 minutes.

While coherent precipitation occurs, two types of heterogeneous precipitation concurrently proceed as depicted in Figure 5. One type is a cellular decomposition resulting in α ferrite and β-Mn phases. The other is a grain boundary precipitation of κ carbide. It is worth mentioning that the intercellular regions made up of zones in a TE micrograph (Figure 3) appear as a network of continuous narrow bands in a scanning electron micrograph (Figure 5), which is of lower magnification and, thus, of lower resolution.

Aging at 923 K does not induce line broadening in Figure 6. No κ' phase diffraction lines are evident in the diffraction pattern of a 923 K aged specimen. Only lines of α, β-Mn, and κ carbide are present without any sign of intermediate phase precipitation. Precipitation of β-Mn occurs only after prolonged aging for 1.9×10^4 minutes. One can note that β-Mn precipitation is more substantially retarded at 923 K than at 823 K.

2. *Alloy B*

In contrast to the aforementioned line broadening observed in the 823 K aging of alloy A, the sidebands flanking each austenite diffraction line appeared in the initial stage of aging of alloy B at 823 K. Figure 7 shows the sequential changes in X-ray diffraction patterns revealing the sidebands around the {200} parent austenite diffraction line. The present sideband observation supports Storchak and Drachinskaya's similar X-ray observation[9] in a single crystal Fe-28 wt pct Mn-9 wt pct Al-0.9 wt pct C alloy, and indicates that zones are formed periodically in the whole matrix[15–20] to result in the modulated structure. Evidence of this is given in Figure 8. A homogeneous lattice modulation occurs throughout the matrix in each grain (Figure 8(a)), and a uniform wave-like contrast is obtained under the operating g_{200} in the (002) matrix plane (Figure 8(b)), indicating the {100} structural modulation. Hereafter, we refer only to the diffraction profile around the $\{200\}_\gamma$ line at various stages (Figure 7) to describe the coherent matrix precipitation.

On further aging, sidebands move toward the fundamental $\{200\}_\gamma$ line, which is the natural consequence of growth of the modulated structure.[15–20] It is worth noting the sharp peak profile and fixed angular position of the $\{200\}_\gamma$ line at this stage. On further aging, near the maximum of the low-angle sideband, an additional diffuse line begins to appear, and, at the same time, the high-angle sideband intensity abruptly increases (4.3×10^3 minutes aging). Most likely, a diffuse line appears because of formation of the metastable κ' phase, and the sudden intensity increase of the high-angle sideband is caused by depletion of solute atoms in the austenite. This stage thus seems to correspond to a transitional stage at which the modulated structure gives way to a two-phase structure. One can note again that the peak profile and angular position of the $\{200\}_\gamma$ line still remains unchanged. After prolonged aging for 2.2×10^4 minutes, the sidebands, as well as the parent $\{200\}_\gamma$ line, disappear. The resulting profile reveals only two sets of diffraction lines corresponding to the respective phase, and is similar to that of 3.0×10^4 minutes of aged alloy A (Figure 2). This similarity further reflects that the modulated

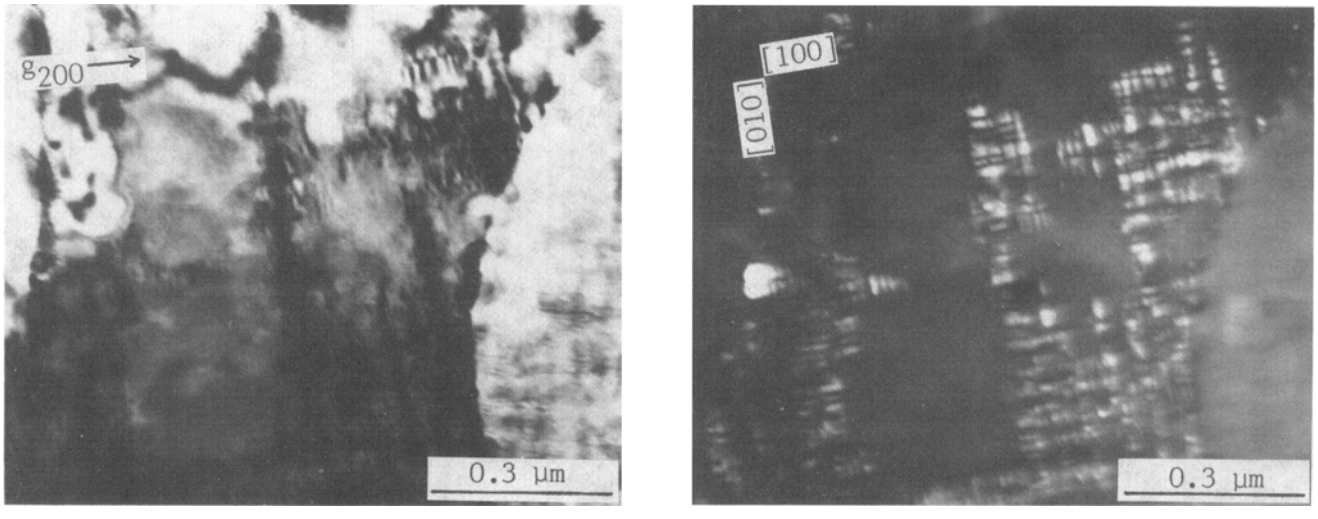

(*a*) (*b*)

Fig. 4—Transmission electron micrographs of alloy A after aging at 823 K for 1.5×10^4 min: (*a*) bright-field image; (*b*) dark-field image from the (100) superlattice spot. Foil normal near [001].

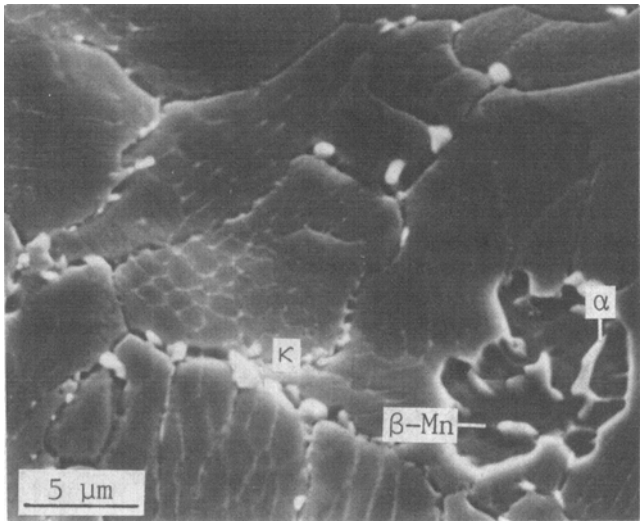

Fig. 5—Scanning electron micrograph of alloy A after aging at 823 K for 3.6×10^3 min. Note that the intercellular regions containing zones (Fig. 3) appeared as a network of narrow bands due to low resolution.

structure evolves into a two-phase structure at this stage. However, prior to formation of κ carbide in the matrix, competing heterogeneous precipitation reactions similar to those occurring in alloy A (Figure 9) seem to become the dominant mode of the decomposition process.[12]

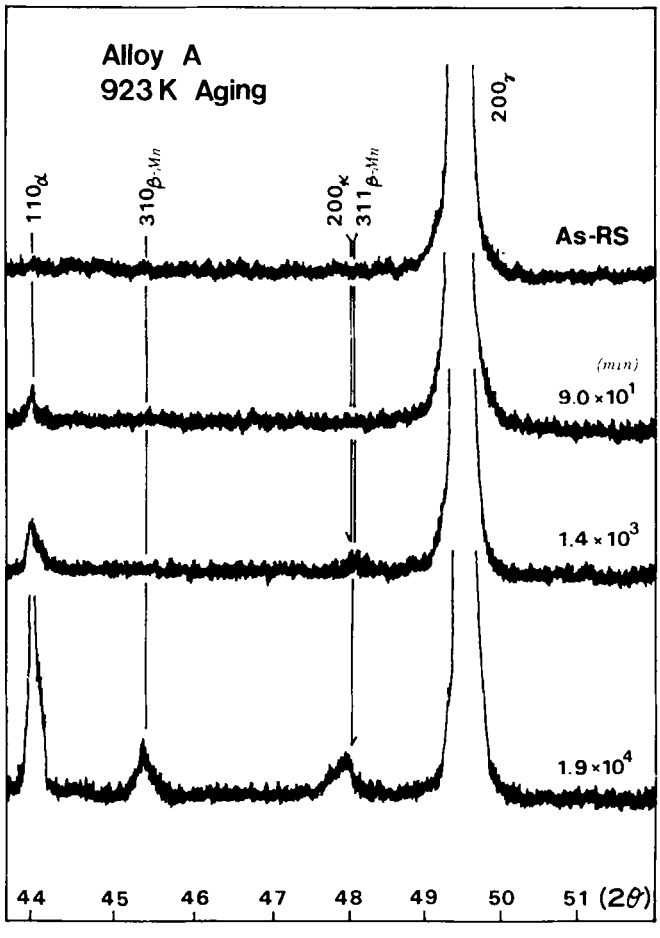

Fig. 6—Sequential changes in the X-ray diffraction pattern of alloy A on aging at 923 K.

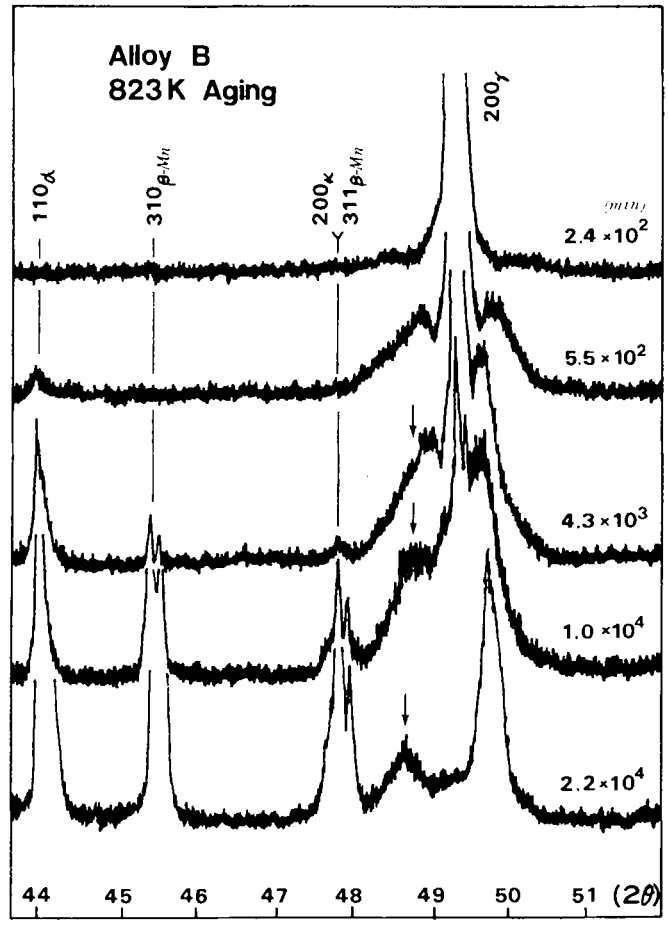

Fig. 7—Sequential changes in the X-ray diffraction pattern of alloy B on aging at 823 K. Arrows indicate the diffraction lines of metastable κ' phase.

In specimens aged at 923 K, however, the X-ray sideband phenomenon ceases to occur. Instead, line broadening of the fundamental austenite diffraction lines is observed (Figure 10). This aging behavior manifested in the X-ray diffraction is similar to that of alloy A aged at 823 K. To clarify the similar pattern development in the X-ray diffraction results, we have conducted TEM investigations. In Figure 11, zones enclosed inside the bands are evident, instead of the modulated structure which tends to cover the whole grain (Figure 8). Zone formation of alloy B at 923 K is consistent with line broadening of X-ray fundamental lines. In Figure 11, {100} zones are distinctively aligned along the [100] direction inside a characteristic group of bands. This microstructural morphology is somewhat different from what is displayed by alloy A on aging at 823 K. Although there is a slight morphological difference between the microstructures of alloy A aged at 823 K and alloy B aged at 923 K, one feature is common between the two: line broadening of X-ray fundamental lines is caused by zone formation. The matrix precipitation proceeds to the conclusion, with κ carbide and retained austenite as the final products. Figure 12 shows carbides that formed in the matrix after prolonged aging for 2.0×10^4 minutes. As observed in the 923 K aging of alloy A, β-Mn precipitation is also retarded at this temperature, and it is detected only after prolonged aging.

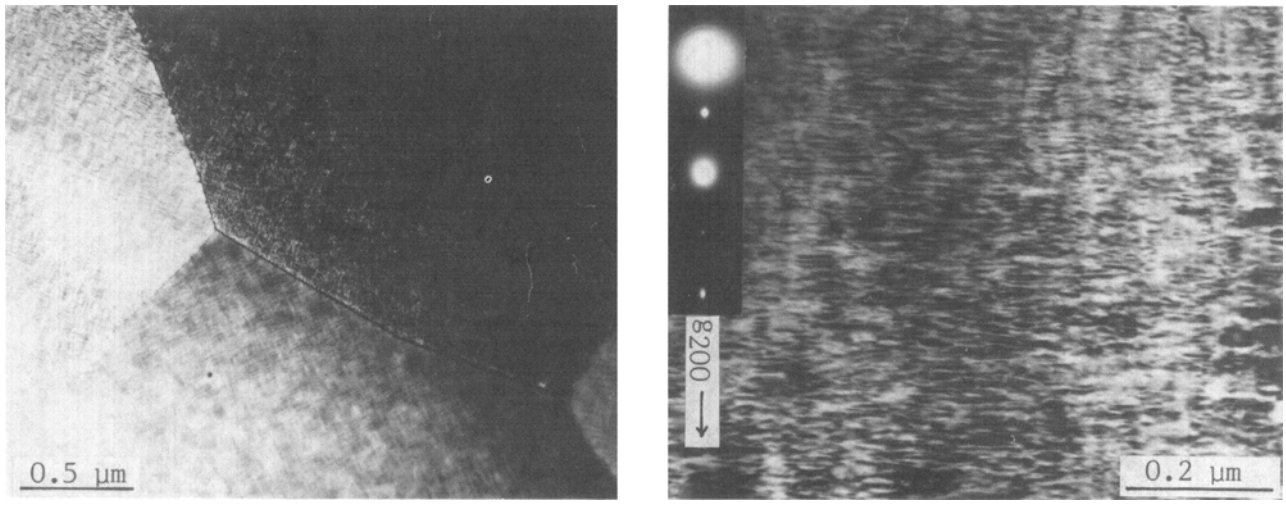

Fig. 8—Bright-field transmission electron micrographs of alloy B after aging at 823 K for 3.0×10^3 min: (*a*) low magnification; (*b*) high magnification. Foil normal of (b) near [001]. Note the (100) superlattice spot inserted in (b), indicating that fcc-based ordering occurred in the solute-rich zone of the modulated structure.

IV. DISCUSSION

A. *Solidification Structure*

A feature of RS austenitic Fe-base alloys is that their structure varies, with the increasing cooling rate, from dendritic or cellular to segregation-free grain microstructure.[13,21] Hayzelden *et al.*[21] have described the cooling rate dependence of the RS microstructure in terms of the degree of undercooling before the onset of solidification in melt-spun Fe-Ni austenitic alloys. For instance, under large undercooling of the melt far below the critical temperature T_o where the free energies of liquid and solid coincide, segregation-free homogeneous columnar grains can form first from the chill-block contact side by massive solidification. Then, due to adiabatic recalescence, thermal dendrite or cellular breakdown is said to result, respectively, in the convoluted grain boundary or internal cell structure near the reverse side of the ribbon. In a similar manner, because of non-Newtonian cooling

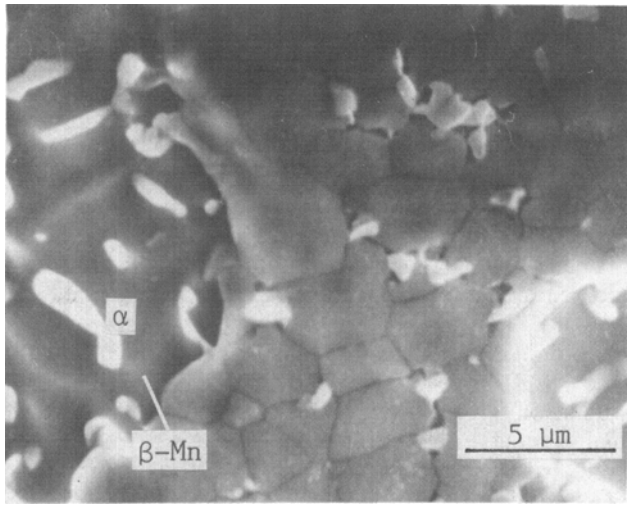

Fig. 9—Scanning electron micrograph of alloy B after aging at 823 K for 4.3×10^3 min.

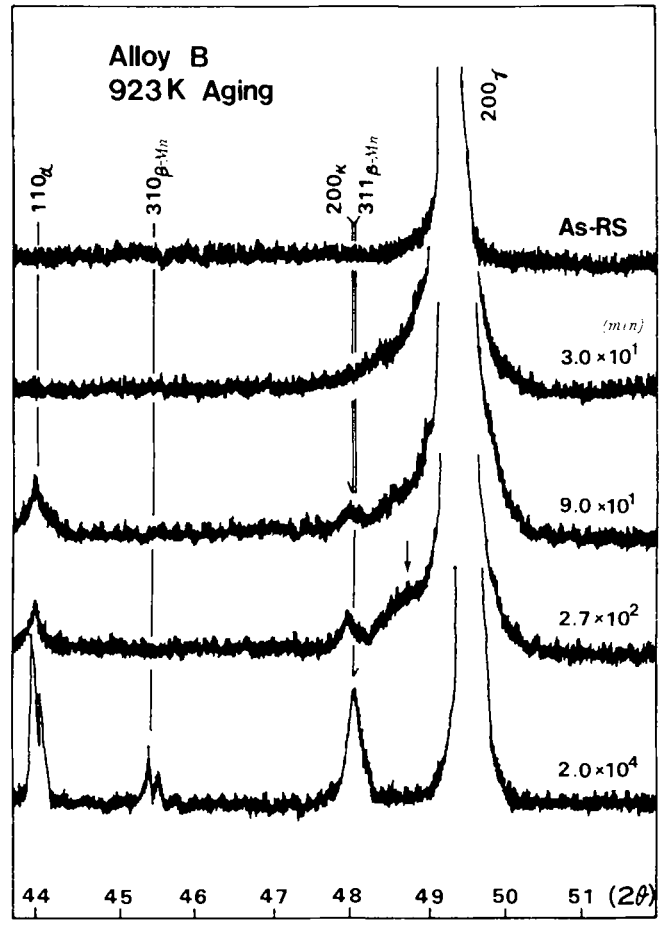

Fig. 10—Sequential changes in the X-ray diffraction pattern of alloy B on aging at 923 K. Arrow indicates the diffraction line of metastable κ′ phase.

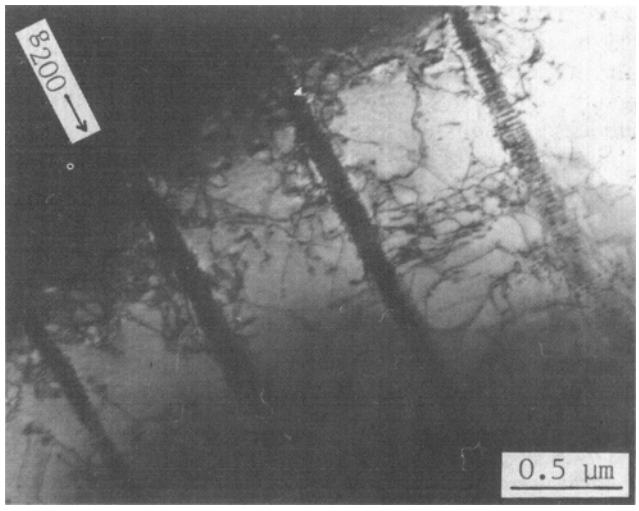

Fig. 11—Bright-field transmission electron micrograph of alloy B after aging at 923 K for 9.0×10^1 min. Foil normal near [011].

during RS, the RS structure may differ from the chill-block contact side to the reverse side of the ribbon. From this viewpoint, it is believed that there might be certain differences in the RS structure between the chill-block contact and reverse sides of ribbons of the present RS alloys A and B. However, as evident from the microstructural features of as-rapidly solidified and aged alloys so far presented, the grains of our alloys are not homogeneous. In particular, the RS structure of alloy A is essentially cellular dendritic. This, in turn, implies that the cooling rate imposed was insufficient to undercool the melts of alloys A and B far enough below the respective critical temperature to induce massive solidification. In addition, judging from the cellular solidification structure revealed in the aged specimens (Figures 3 and 11), the cell growth occurred in the $\langle 100 \rangle_\gamma$ directions. Another possible explanation for the complex microstructural feature of our alloys may stem from the instability of austenitic phase at the actual solidification temperature.

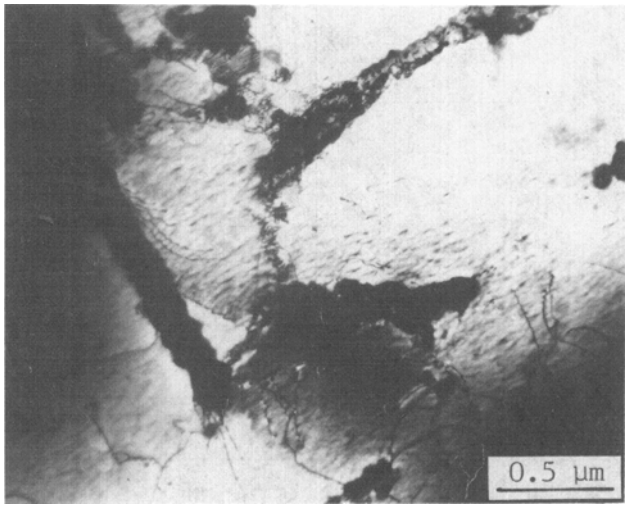

Fig. 12—Bright-field transmission electron micrograph of alloy B after aging at 923 K for 2.0×10^4 min.

The fact that the diffusion rate of the interstitial carbon atoms is much higher than that of substitutional atoms, such as Mn and Al, points to the fact that the main segregating element might be carbon. Possible evidence can be found in the previous works[23,24] on the RS of carbon-containing ferrous alloys, in which preferential precipitations of carbide phases, such as $M_{23}C_6$ and M_2C, were observed at solute-segregated intercellular or interdendritic regions that took place after aging and even during the RS process. This also can be related to some carbon redistribution across the liquid/solid interface in the solidification stage.

B. *Matrix Precipitation*

It has been shown that line broadening occurs in 823 K aging of alloy A and in 923 K aging of alloy B, and it is related to the nonuniform zone formation at the solute-segregated intercellular regions, whereas the sideband phenomenon, occurring in 823 K aging of alloy B, originates from formation of the uniformly periodic zone alignment in the modulated structure throughout the whole grain. Remembering that the only difference between alloys A and B is the carbon content, we may conjecture that carbon segregation along the intercellular boundaries, together with matrix carbon supersaturation in the RS specimen, affects the initial decomposition mode. Carbon concentration fluctuation is certainly envisioned, and {100} lattice modulation, due to formation of periodic carbon-rich zones separated by carbon-poor zones under the carbon supersaturation condition, is expected as a result (823 K aging of alloy B). The somewhat developed carbon-rich zones take cuboidal shape rather than the platelet one as opposed to the suggestions made by Krivonogov *et al.*[8] and Storchak and Drachinskaya[9] (Figure 4).

A phenomenological correlation between X-ray sidebands and modulated structure goes hand in hand from the diffraction theory point of view. We first assume that each carbon-rich zone in the {100} modulated structure is located at a macrolattice point which is the center of a microregion of composition fluctuations. If we can neglect the atomic scattering factor variation, then the X-ray intensity from a crystal with the perfectly periodic arrangement of zones in one dimension, *i.e.*, due to one-dimensional structural modulation, can be expressed as $I_t(g) = I_p(g)I_u(g)$ ($g = 2\sin\theta_B/\lambda$: θ_B = Bragg diffraction angle and λ = X-ray wavelength), where $I_p(g)$ is the Laue interference function for the crystal of the imaginary macrolattice, *i.e.*, $\sin^2(gNQa)/\sin^2(gQa)$ (N = number of imaginary macrolattice, Qa = modulation wavelength, and a = lattice parameter of the parent austenite phase), and $I_u(g)$ represents the intensity from one unit microregion.[15] $I_u(g)$ may take various functional forms, depending on the model of structural modulation, such as a sinusoidal wave,[18] a rectangular wave,[19] or a 3-phase model,[15] in which a part of the matrix is assumed to be untransformed. If N is sufficiently large, the sharp maximum will be allowed at reciprocal lattice positions, $g = h/a \pm p/Qa$, where h corresponds to the index of the Bragg diffraction line, and p is the subsidiary order for the sideband reflection.[15,18,19] However, only the first order of sidebands ($p = 1$), with diffuse peak profile, is

observed for low index lines (Figure 7, for example). Furthermore, the sidebands are asymmetric in position and intensity in many cases.[15,19]

Tsujimoto *et al.*[15] attempted to interpret the diffuseness and asymmetry of the sidebands in terms of the degree of long periodicity of the modulation: For this, they introduced an interference function $I_d(g)$ for a crystal with unit microregions of disturbed periodicity instead of $I_p(g)$: $I_t(g) = I_d(g)I_u(g)$. This seems to be a somewhat arbitrary simplification since the changes in $I_u(g)$ are not taken into account. In spite of this and although they did not obtain the exact functional form of $I_d(g)$, they could show that, with increasing disturbance in periodicity, $I_d(g)$ became broader, so that the resulting sidebands became increasingly diffuse. This may also be understood in terms of superposition of modulations with different wavelengths. The peak profile and angular positions of the main Bragg lines, however, would not be substantially changed, since their allowed diffraction positions are essentially independent of the modulation wavelengths, Qa, in contrast to those for the sideband reflections, as previously noticed in Figure 7. On the other hand, in an extreme case when a random zone arrangement is assumed, there cannot be any prominent sideband interference coming from the unit regions, so that the pattern may appear to be governed by $I_u(g)$ rather than $I_p(g)$. This is, in fact, the case of the random zone model suggested by Guinier.[24] Since $I_u(g)$ represents the intensity from one unit microregion, assuming the small zone size and lattice mismatch therein, it becomes apparent in this extreme case that the main Bragg lines become broadened, instead of separate diffuse reflections like the sidebands. Furthermore, if $I_u(g)$ is not symmetric with respect to the position of the main Bragg line ($g = h/a$), owing to asymmetry in the fluctuating strain amplitudes for the solute-rich and solute-poor zones inherited from the difference in their volume fractions, then the broadening of the main Bragg line accordingly will be asymmetric.

In the above, we considered the change of the type of diffuse reflections that could occur *via* disturbed periodicity in the arrangement of zones formed uniformly in the matrix. However, the present observations of the microstructures being responsible for line broadening are rather complex, as seen in Figure 3, in which zones are shown to form preferentially at the intercellular regions, and, in addition, their long-period periodicity changes from the exterior to interior intercellular regions, owing to some gradient of solute segregations across those regions. Accordingly, the actual scattering is imagined to take place in the more complicated manner; but the resulting pattern of the main Bragg line broadening suggests that such breaking of zone periodicity by intercellular regions within a grain may be regarded as aforementioned random zone arrangement on the whole by the diffracted beam.

The observed structural modulation in the $\langle 100 \rangle_\gamma$ directions indicates that the elastic anisotropy ratio, $A = 2C_{44}/(C_{11} - C_{12})$, is greater than unity[25,26] in the Fe-Mn-Al-C austenite phase as in other fcc- and bcc-based sideband alloys, such as Cu-Ni-Fe,[16,27] Cu-Ti,[17,28] Ni-Ti,[29] and Fe-Mo.[30] This, in turn, implies that composition fluctuations have occurred along the elastically-soft $\langle 100 \rangle_\gamma$ directions, and further suggests that the spinodal decomposition[25] is likely to be responsible for the initial homogeneous formation of the modulated structure in RS alloy B at 823 K. The growth rate of the modulated structure was examined by determining the modulation wavelength as a function of the aging time from the well-known Daniel-Lipson formula,[18] for which we used the sidebands belonging to the $\{200\}_\gamma$ Bragg line. Figure 13 shows a log-log plot of the modulations *vs* aging time, from which it is found that a kinetic relationship $\lambda = kt^{1/2.8}$ is obeyed in the growth stage of the modulated structure for alloy B at 823 K. When the modulation wavelength reached about 25 nm, the modulated structure started to break down. It is reckoned that the carbon-rich zones transform to metastable κ' phase, resulting, probably, in the raft structure similar to the one seen in Figure 4, conjecturing further from Krivonogov *et al.*'s TEM observation of epitaxial (interfacial) dislocations,[8] of which formation can reduce the strain energy created by the lattice mismatching.[31] This may be linked to loss of coherency of κ' carbide. However, clarification of this structural change will need a separate, in-depth, high resolution TEM study. Granting the matrix precipitation of the equilibrium κ carbide phase at the final stage as evidenced in Figure 12, the overall sequence of the matrix precipitation process under the high carbon supersaturation condition (823 K aging of alloy B) can be summarized as follows:

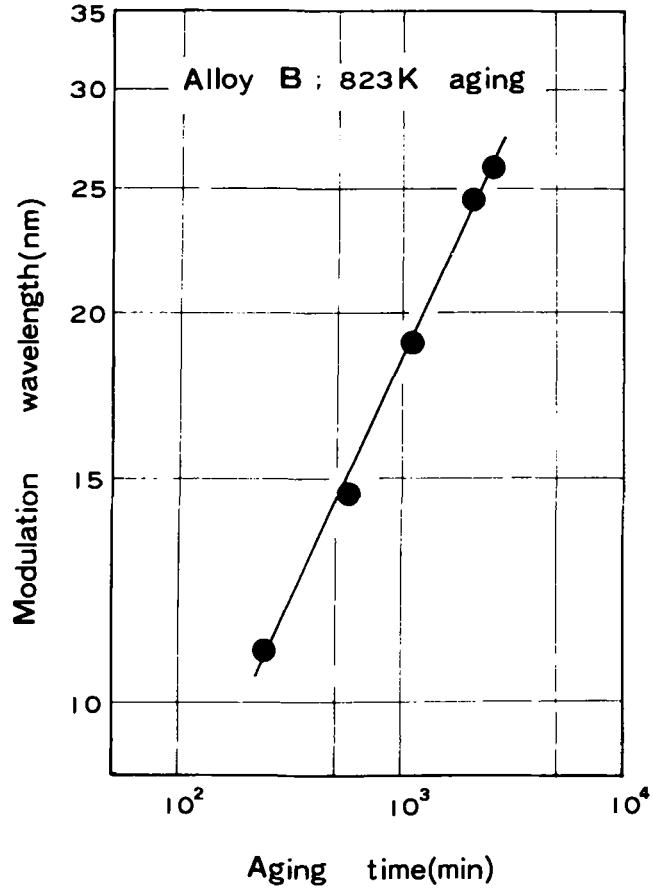

Fig. 13—Modulation wavelength *vs* aging time curve of 823 K aged alloy B on the log-log scale.

$$\text{supersaturated } \gamma \rightarrow \{100\} \text{ structure modulation consisting of carbon-rich and carbon-poor zones}$$
$$\rightarrow \text{coherent or partly coherent } \kappa'\text{-phase having } \{100\} \text{ habit planes}$$
$$\rightarrow \text{equilibrium } \kappa \text{ carbide, } (Fe,Mn)_3\,AlC_x$$

So far we have been concerned only with clustering of carbon atoms in the initial decomposition stage; but observation of superlattice reflections from carbon-rich zones and/or κ'-phase indicates that the initial clustering and subsequent formation of κ' involve ordering reactions as in Cu-Ti[17,28] and Ni-Ti.[29] Considering fcc-based ordering reactions and, further, taking into account a cooperative ordering of aluminum and carbon atoms in RS Ni_3Al-xC pseudobinary alloys,[32] it is likely that the initial and subsequent decomposition processes together involve ordering of aluminum atoms coupled with their clustering, finally leading to the $L'1_2$ ordered structure of $(Fe,Mn)_3\,AlC_x$ chemical formula of the κ carbide. From the results in this study, it can also be stated that the solvus temperature of the modulated structure lies between 823 and 923 K for alloy B, whereas that for alloy A lies at a temperature below 823 K.

C. *Grain Boundary Precipitations*

A distinct difference in the heterogeneous grain boundary precipitation pattern of the RS and conventionally quenched alloys is that the reaction proceeds much faster in the RS alloys than in the conventionally quenched alloys.[12] This may simply be attributed to the much larger grain boundary areas, which can act as heterogeneous nucleation sites in the RS alloys more so than in conventionally quenched alloys. The grain boundary precipitations of κ carbide and β-Mn phase were previously observed in a conventionally quenched and aged alloy[8] whose composition is similar to ours. In their work,[8] Krivonogov *et al.* reported that the precipitation of β-Mn phase was so sluggish that it was observed only after very prolonged aging at temperatures between 923 and 1023 K, and they suggested that the β-Mn phase precipitated initially in the solute-depleted austenite regions that formed as a consequence of κ carbide precipitation, *i.e., via* a reaction, solute-depleted austenite $\rightarrow$ β-Mn + α. In the meantime, in our RS alloys A and B, β-Mn precipitation occurred at 923 K after prolonged aging for about 10^4 minutes as in the conventionally quenched alloy.[8] However, on aging at 823 K, β-Mn precipitated early at the grain boundaries. The microstructural morphology of the product phases is somewhat unique in that the coprecipitate ferrite particles are immersed in the low melting β-Mn pool (Figures 5 and 9). Then, the colony of the product phases rapidly encroached into the matrix on further aging.

V. CONCLUSION

The results obtained in this study can be summarized as follows:

1. An austenitic single-phase alloy with the cellular dendritic structure was prepared by melt spinning of alloy A. Such microstructure was easily identified by SEM. The as-RS microstructure of alloy B observed by SEM revealed more or less homogeneous austenitic phase, but the formation of precipitate band on aging of RS alloy B connotes the presence of as-RS submicrostructure on a finer scale than that of alloy A.
2. Both RS alloys A and B were found to be age hardenable, but the initial decomposition modes greatly depended both on carbon composition and aging temperature, *i.e.*, the degree of carbon supersaturation. At low-carbon supersaturation (823 K aging of alloy A and 923 K aging of alloy B), {100} zones formed. In alloy A, the zones preferentially formed along the intercellular boundaries of the RS structure. In alloy B, they formed in crystallographically oriented bands, preferentially aligned in the ⟨100⟩ directions on aging. In the aged alloys in the low carbon supersaturation condition, only line broadening was observed in the X-ray pattern. In contrast, at high supersaturation (823 K aging of alloy B), a modulated structure consisting of alternate carbon-rich and carbon-poor zones periodically aligned in the $\langle 100 \rangle_\gamma$ directions was formed. The X-ray sidebands and TE micrographs both prove their existence.
3. The initial formation of the modulated structure in 823 K aging of alloy B is most likely to occur *via* the spinodal mechanism. The growth rate of the modulated structure obeyed a kinetic relationship, $\lambda = kt^{1/2.8}$.
4. The solvus of the modulated structure lies between 823 and 923 K for alloy B, but it lies at temperatures below 823 K for alloy A.
5. Both the line broadening and the sideband reflections observable in the early stage of aging give way to the same diffraction profile emanating from two-phase structure of the metastable phases in the next stage of aging. The metastable κ' showed the {100} habit plane.
6. Both the carbon-rich zone and metastable κ'-phase are of an ordered fcc structure. However, there are differences in the degree of alloy ordering and composition between the two.
7. The final stage of the matrix precipitation of κ carbide was observed only after prolonged aging of alloy B at 923 K. In other cases, the ensuing competing grain boundary reactions seemed to finalize the decomposition process: the grain boundary precipitation of the κ carbide and β-Mn precipitation. In particular, β-Mn precipitation occurred cooperatively with precipitation of ferrite in a degenerated cellular mode and then proceeded rapidly, encroaching the matrix at 823 K.

Note Added in Proof

A paper concerned with TEM observation of the modulated structure in Fe-Mn-Al-C austenitic alloys prepared by the conventional process has been published by the present authors during the revision of this paper (K.H. Han, J.C. Yoon, and W.K. Choo: "TEM Evidence of Modulated Structure in Fe-Mn-Al-C Austenitic Alloys," *Scripta Metallurgica*, 1986, vol. 20, no. 2, pp. 33-36). In the paper, the structural modulation in the ⟨100⟩

directions has been presented as well as *in situ* sideband formation in the reciprocal space. In addition, from the analysis of the observed superlattice spots, we reasoned that the fcc-based ordering in the carbon-rich zones corresponded to the $L'1_2$ type ordering, leading to an ordered crystal structure similar to that of the κ carbide, $(Fe,Mn)_3AlC_x$. It was further suggested from the evidences of the initial homogeneous (continuous) decomposition that phase decomposition began *via* the spinodal decomposition. These results are consistent with the present observations of initial decomposition of alloy B at 823 K in this paper.

ACKNOWLEDGMENTS

The authors would like to thank Korea Advanced Institute of Science and Technology for financial assistance for this study. A part of this study (TEM study) was carried out under a grant by the Korea Science and Engineering Foundation. The authors appreciate the review committee's helpful suggestions. Without them, this paper would only have been written based on the SEM and X-ray diffraction data.

REFERENCES

1. J.L. Ham and R.E. Cairns: *Product Eng.*, 1958, vol. 29, no. 12, pp. 50-52.
2. D.J. Schmatz: *Trans. ASM*, 1960, vol. 52, pp. 898-913.
3. S.K. Banerji: *Metal Progr.*, 1978, vol. 113, no. 4, pp. 59-62.
4. R. Wang and F.H. Beck: *Metal Progr.*, 1983, vol. 123, no. 4, pp. 72-76.
5. P.J. James: *J. Iron Steel Inst.*, 1969, vol. 207, pp. 54-57.
6. G.L. Kayak: *Met. Sci. Heat Treat.*, 1969, no. 2, pp. 95-97.
7. M.F. Alekseyenko, G.S. Krivonogov, L.G. Kozyreva, I.M. Kachanova, and L.V. Arapova: *Met. Sci. Heat Treat.*, 1972, no. 3, pp. 187-89.
8. G.S. Krivonogov, M.F. Alekseyenko, and G.S. Solov'yeva: *Phys. Met. Metallogr.*, 1975, vol. 39, no. 4, pp. 86-92.
9. N.A. Storchak and A.G. Drachinskaya: *Phys. Met. Metallogr.*, 1977, vol. 44, no. 2, pp. 123-30.
10. A. Inoue, Y. Kojima, T. Minemura, and T. Masumoto: *Metall. Trans. A*, 1981, vol. 12A, pp. 1245-53.
11. K.H. Han and W.K. Choo: *Metall. Trans. A*, 1983, vol. 14A, pp. 973-75.
12. W.K. Choo and K.H. Han: *Metall. Trans. A*, 1985, vol. 16A, pp. 5-10.
13. J.V. Wood and R.W.K. Honeycombe: *J. Mater. Sci.*, 1974, vol. 9, pp. 1183-88.
14. E.S.U. Laine, E.J. Hiltunen, and M.H. Heinonen: *Acta Metall.*, 1980, vol. 28, pp. 1565-69.
15. T. Tsujimoto, K. Hashimoto, and K. Saito: *Acta Metall.*, 1977, vol. 25, pp. 295-303.
16. E.P. Butler and G. Thomas: *Acta Metall.*, 1970, vol. 18, pp. 347-65.
17. D.E. Laughlin and J.W. Cahn: *Acta Metall.*, 1975, vol. 23, pp. 329-39.
18. V. Daniel and H. Lipson: *Proc. Roy. Soc. (London)*, 1943, vol. 181A, ser. A, pp. 368-78.
19. E. Biedermann: *Acta Cryst.*, 1960, vol. 13, pp. 650-52.
20. B. Ditchek and L.H. Schwartz: *Ann. Rev. Mater. Sci.*, 1979, vol. 9, pp. 219-53.
21. C. Heyzelden, J.J. Rayment, and B.B. Cantor: *Acta Metall.*, 1983, vol. 31, pp. 379-86.
22. J.V. Wood and R.W.K. Honeycombe: *Mater. Sci. Eng.*, 1976, vol. 23, pp. 107-12.
23. I.R. Sare and R.W.K. Honeycombe: *Met. Sci.*, 1979, vol. 13, pp. 269-79.
24. A. Guinier: *Acta Metall.*, 1955, vol. 3, pp. 510-12.
25. J.W. Cahn: *Acta Metall.*, 1962, vol. 10, pp. 179-83.
26. A.G. Khachaturyan: *Phys. Status Solidi*, 1969, vol. 35, pp. 119-32.
27. R.J. Livak and G. Thomas: *Acta Metall.*, 1971, vol. 19, pp. 497-505.
28. A. Datta and W.A. Soffa: *Acta. Metall.*, 1976, vol. 24, pp. 987-1001.
29. D.E. Laughlin: *Acta Metall.*, 1976, vol. 24, pp. 53-58.
30. T. Miyazaki, S. Takagishi, H. Mori, and T. Kozaki: *Acta Met.*, 1980, vol. 28, pp. 1143-53.
31. D. de Fontaine: *Acta Metall.*, 1969, vol. 17, pp. 477-82.
32. K.H. Han and W.K. Choo: *Scripta Metall.*, vol. 17, pp. 281-84.